RSC Advances

PAPER

View Article Online
View Journal | View Issue

Cite this: *RSC Adv.*, 2022, **12**, 20037

Using a two-step method of surface mechanical attrition treatment and calcium ion implantation to promote the osteogenic activity of mesenchymal stem cells as well as biomineralization on a β-titanium surface

Run Huang, *[abc] Yufei Hao,[a] Yusong Pan, [a] Chengling Pan,[ab] Xiaolong Tang,[bd] Lei Huang,[e] Chao Du,[a] Rui Yue[a] and Diansheng Cui[e]

Surface treatment is known as a very efficient measure by which to modulate the surface properties of biomaterials in terms of grain structure, topography, roughness and chemistry to determine the osseointegration of implants. In this work, a two-step method of surface modification was employed to impart high osteogenic activity and biomineralization capacity on a Ti–25Nb–3Mo–2Sn–3Zr alloy (a type of β-titanium named TLM). The preliminary surface mechanical attrition treatment (SMAT) refined the average grain size from 170 ± 19 μm to 74 ± 8 nm in the TLM surface layer and promoted the surface to be much rougher and more hydrophilic. The subsequent Ca-ion implantation did not change the surface roughness and topography obviously, but enhanced the surface wettability of the SMAT-treated TLM alloy. The *in vitro* evaluations of the adhesion, proliferation, osteogenic genes (RUNX2, ALP, BMP-2, OPN, OCN and COL-I) and protein (ALP, OPN, OCN and COL-I) expressions, as well as extracellular matrix (ECM) mineralization of mesenchymal stem cells (MSCs) revealed that the initial SMAT-treated sample significantly enhanced the adhesion and osteogenic functions of MSCs compared to an untreated TLM sample, and the subsequent introduction of Ca ions onto the SMAT-derived nanograined sample further promotes the MSC adhesion, proliferation, osteo-differentiation and ECM mineralization due to the adsorption of more proteins such as laminin (Ln), fibronectin (Fn) and vitronectin (Vn) on the surface, as well as the increase in extracellular Ca concentrations. In addition, the biomineralization capacity of the samples was also evaluated by soaking them in simulated bodily fluid (SBF) at 37 °C for 28 days, and the results showed that the Ca-ion implanted sample significantly boosted the deposition of Ca and P containing minerals on its surface, which was associated with the generation of more Ti–OH groups on the surface after ion implantation. The combination of the SMAT technique and Ca-ion implantation thus endowed the TLM alloy with outstanding osteogenic and biomineralization properties, providing a potential means for its future use in the orthopedic field.

Received 4th January 2022
Accepted 27th June 2022

DOI: 10.1039/d2ra00032f

rsc.li/rsc-advances

1. Introduction

In recent years, titanium-based metals have attracted extensive attention for the fabrication of dental and orthopedic implants used in clinic, mainly due to their good mechanical properties and biocompatibility.[1–3] However, the limited osseointegration of titanium-based metals to its surrounding bone tissue and the long healing period after their implantation still brings too much discomfort and economic pressure to patients.[2,4,5] In this regard, long lasting and strong bonding between the implant and bone should be established for increasing the surgical success rate and lifetime of titanium-based implants.

It is widely known that modulating surface properties, including roughness,[6,7] topography,[8] grain structure,[9,10] and chemistry,[11–13] is a very effective measure to improve the osseointegration of an implant as the surface characteristics of biomaterials play an important role in determining the early cellular behavior at the implant/tissue interface during the healing process.[14] Hence, surface modification provides

[a]*School of Materials Science and Engineering, Anhui University of Science and Technology, Huainan 232001, China. E-mail: runhuang@aust.edu.cn; Fax: +86 0554 6668201; Tel: +86 0554 6668201*

[b]*Institute of Environment-friendly Materials and Occupational Health of Anhui University of Science and Technology (Wuhu), Wuhu 241003, China*

[c]*Anhui International Joint Research Center for Nano Carbon-based Materials and Environmental Health, Anhui University of Science and Technology, Huainan 232001, China*

[d]*Medical School, Anhui University of Science and Technology, Huainan 232001, China*

[e]*Department of Gastrointestinal Surgery, Hubei Cancer Hospital, Wuhan 430060, China*

a potential avenue to enhance the biological performance, simultaneously preserving the outstanding bulk properties of titanium-based implants.[15] There are various routes by which to modify titanium-based metals by monitoring surface roughness, topography or grain structure to achieve good biological properties, such as etching,[16,17] sandblasting,[18] shot peening[19] and sliding friction treatment (SFT).[20] Among them, nanograined titanium-based surfaces with microroughness generated by the surface mechanical attrition treatment (SMAT) approach have been utilized effectively to benefit cell response *in vitro*[21–24] and enhance bone formation capacity *in vivo*.[25] For instance, Zhao *et al.* verified that SMAT-processed pure titanium with increased surface roughness and refined grains promoted the adhesion, viability, and proliferation of osteosarcoma cells.[26] Lai *et al.* also attributed enhanced mesenchymal stem cells (MSC) adhesion, proliferation, and osteo-related gene expression on SMAT-treated pure titanium sheets to their surface roughening and nanocrystallization.[27] Our previous reports even demonstrated that the sole grain refinement in the surface layer of a β-titanium alloy induced by SMAT remarkably improved cell–material interactions.[9,28] Therefore, the SMAT technique shows good potential to endow titanium and its alloys with enhanced biological activity by regulating their surface properties in terms of roughness, topography, and grain structure.

Surface chemistry also plays an important role in influencing the cell response and subsequent quality of new tissue bonding to the implants. Bioactive metallic-elements such as zinc (Zn), magnesium (Mg), calcium (Ca) and strontium (Sr) were introduced onto biomedical materials by various methods, and their positive effect on the amelioration of the biological property was proved.[29–32] One commonly used technique to introduce these metallic elements onto titanium-based implants is ion implantation, a means by which target ions can be injected into the surface region of metals without altering their surface topography/morphology.[4,33] As the most abundant metallic element in the human body, Ca mainly stored in bone was reported to have a significant influence on the maturation of osteoblasts and mineralization of bone tissue.[34,35] Previous investigations that have adopted ion implantation to introduce Ca ions onto titanium-based metals have found that modified surfaces accelerated the precipitation of calcium phosphate while soaked in simulated bodily fluids[36–39] and promoted adhesion,[40] spread,[41] proliferation,[42] certain bone-associated gene expression[43] and modulated the progression of the cellular cycle[15] of MG-63 cells, as well as benefiting the attachment and biocompatibility-related gene expression of MC3T3-E1 cells.[33] Apart from osteoblastic cell lines, Won *et al.* found that ion implantation of Ca ions onto a titanium surface benefited the initial attachment of bone marrow MSCs.[44] MSCs were reported to exhibit self-renewal and multi-lineage differentiation potential, and their *in vitro* expansion and osteogenic differentiation capability were considered to be a key element that directly determined whether or not the biometals could achieve successful osseointegration after implantation.[34,45] Despite that, it is worth noting that the aforementioned available literature mainly focused on cell response and biomineralization on pure Ti and Ti6Al4V (mainly stabilized as α phase), whereas, actually, it is more meaningful to investigate the behavior of stem cells and biomineralization on Ca-ion implanted β-Ti metals, as β-Ti exhibits a much lower elastic modulus than α-Ti,[46,47] and therefore has been considered to be able to much better overcome the "stress shielding" effect related to the mismatching of the elastic modulus between the implants and the surrounding hard tissue.[2,48]

In this study, to endow Ti–25Nb–3Mo–2Sn–3Zr (TLM), a new β-titanium alloy, with excellent osteogenic functions and biomineralization ability, a two-step method of combining SMAT and Ca-ion implantation surface treatments was employed to regulate the surface characteristics of the alloy. The changes in surface properties resulting from the SMAT and ion implantation were assessed, and the synergistic effects of surface roughening, grain refinement, and Ca ions on the protein adsorption and rabbit bone MSCs were explored *in vitro*. Meanwhile, the biomineralization capacity of different samples was also evaluated *via* simulated bodily fluid (SBF) immersion experiments. The implantation of Ca ions onto a SMAT-achieved nanograined surface was identified to be able to endow the TLM alloy with outstanding osteogenic and biomineralization properties, providing an alternative means by which to design titanium implants that exhibit improved clinical performance.

2. Materials and methods

2.1. Sample preparation

TLM plates with dimensions of $\phi 100 \times 3$ mm were selected as the raw material in this study. As a β-type titanium alloy, the nominal composition of TLM alloy is Ti–25Nb–3Mo–2Sn–3Zr (wt%), and the reported β transus temperature is around 710–720 °C.[46] The obtained TLM plates were soluted at 800 °C for 1 h, and then polished to a mirror finish with sandpapers. After that, a portion of the soluted TLM plates were treated using a SMAT machine on one side to refine the grains in the surface layer of the substrates, as described elsewhere.[47,49] In the SMAT process, the diameter of the used stainless-steel balls was 5 mm the vibration frequency was set as 50 Hz, and the treatment was continued for 45 min on each plate at room temperature. Subsequently, the SMAT-treated plates were cut into squares with dimensions of $10 \times 10 \times 3$ mm, and then some of the squares were laid into the chamber of a MEVVA ion implantation device, wherein Ca ions were implanted onto the surfaces of the squares under vacuum state at a pressure of around 1×10^{-5} Pa with a beam energy of 50 keV and a dose of 1×10^{17} ions per cm^2. After Ca-ion implantation, the squares were immediately vacuum-sealed in plastic bags for storage. Thereafter, the above acquired Ca-ion implanted and SMAT-processed squares, together with the squares ($10 \times 10 \times 3$ mm) cut from the soluted plates, were designated as Ca-SMAT-TLM, SMAT-TLM, and TLM samples, respectively.

2.2. Characterization of the surface features

2.2.1. Surface structure and chemical characterization. X-ray diffractometry (XRD, X'Pert PRO, Netherlands) was carried

out to reveal the phase structures of the TLM, SMAT-TLM, and Ca-SMAT-TLM samples. The grain size of the TLM sample was observed under an optical microscope (OM, Reichert MeF3, Germany) and measured by taking the average of the calculation of around 200 grains using the Leica QWIN software. The surface microstructures of the SMAT-TLM and Ca-SMAT-TLM samples were detected by transmission electron microscopy (TEM, JEM-2100, Japan) operated at 200 KeV. To fabricate the TEM foils, the samples were mechanically ground on their untreated sides to obtain thin sheets with a thickness of around 30–50 μm, which were then jet-polished in an electrolyte comprising 90% methanol and 10% perchloric acid. To measure the grain sizes in the surface layer of the samples, about 300 grains from typical TEM photomicrographs were analyzed using a linear intercept method.[50] X-ray photoelectron spectroscopy (XPS, PHI1800, Japan) was performed to determine the surface chemical compositions and depth profiles of the Ca-SMAT-TLM sample, and the sputtering rate was estimated at 8 nm min^{-1}. Additionally, the chemical state of the O element on the different samples was also characterized by XPS and analyzed using the XPS-PEAK41 software. Furthermore, to reveal the surface elemental distribution of the Ca-SMAT-TLM sample, EDS mapping analysis was conducted using a SEM-EDS system (Zeiss Gemini500, Germany).

2.2.2. Surface properties characterization and implanted-ion release. Atomic force microscopy (AFM, SPM-9500J3, Japan) was employed to assess the surface topography and roughness of the TLM, SMAT-TLM, and Ca-SMAT-TLM samples. The typical topography of each surface was determined using a Si_3N_4 probe in non-contact mode, and the roughness of each surface was assessed according to the Ra (average roughness), Rq (root-mean-square roughness), and Rz (10-point maximum height roughness). The scanning area of the AFM measurements was chosen as 25 × 25 μm since the cells (osteoblasts or MSCs) are around 10–50 μm in diameter and their membranes, as well as cell anchoring proteins, have been reported to be very sensitive to surface features with nano-scale irregularity.[51,52] A hydrophilicity instrument (DSA30, Kruss, Germany) was utilized for surface contact angle measurements, where the used liquid was secondary deionized water and the static contact angles were analyzed using the DSA1 software after 5 s of the water droplet making contact with the surface. Three samples from each group were measured to obtain average values.

To explore the implanted Ca-ion release behavior, different samples were incubated in 50 mL of α-Modified Eagle's Medium (α-MEM) containing 10% fetal bovine serum (FBS, Life Technologies, USA) for different immersion times (1, 5, 24, 72, 168 and 336 h) at 37 °C without stirring. At each target time, the leaching solutions from soaked samples were gathered and analyzed by means of inductively coupled plasma-atomic emission spectroscopy (ICP-AES, Optima 3000DV, USA) to determine the concentration of the released Ca ions. Three samples from each group were measured to obtain average values.

The surface adsorption of proteins towards different samples was also measured in α-MEM containing 10% FBS. The adsorbed amounts of laminin (Ln), fibronectin (Fn) and vitronectin (Vn) as well as total proteins after incubation in the medium for 1, 5 and 24 h were determined using the respective ELISA kits at 37 °C. Three samples for each group were tested, and each test was repeated three times ($n = 3$).

2.3. Cell–material interaction studies

2.3.1. Cell culture. Bone mesenchymal stem cells (BMSCs, provided by the medical school at Xi'an Jiaotong University, Xi'an, China) were isolated from the bone marrow of 1 week-old New Zealand rabbits. The obtained BMSCs were then cultured in α-MEM containing 10% FBS and 1% antibiotics at 37 °C under a 5% CO_2 and 95% air atmosphere. The culture medium was changed every 2 days, and only MSCs from passages 3–5 were selected to conduct the cell experiments. A total of 2×10^4 cells suspended in 1 mL of culture medium were seeded in every well of the 24-well plates.

2.3.2. Cell adhesion, proliferation, and morphology. The adhesion and proliferation of MSCs on the TLM, SMAT-TLM, and Ca-SMAT-TLM samples were evaluated using a cell counting kit-8 (CCK-8) assay. The samples were laid centrally in 24-well plates with their treated sides upwards, and cells were seeded on each sample and incubated for 1 h, 5 h, 24 h, 3 days, 7 days, and 14 days. At each prescribed time, the complete medium was discarded, and the samples were washed three times with PBS and then transferred to new 24-well plates. Then, 1 mL of medium containing 100 μL of CCK-8 reagent (Dojindo, Japan) was added to each well and incubated for a further 2 h in the incubator. After that, the cell viability of each sample was measured at an absorbance of 450 nm using a microplate reader. Three replicates for each group were tested, and each test was repeated three times ($n = 3$). Cell adhesion was also evaluated by observing the typical morphology of adherent cells on different samples using SEM. After 5 h of culture, the samples were washed three times with PBS, and fixed with 2.5% glutaraldehyde at 4 °C for 18 h. Dehydration of the cell-fixed samples was then implemented with a series of ethanol solutions (30, 50, 70, 95 and 100%) for 15 min each time. After the samples were further coated with gold, the cell morphology was viewed by FESEM (JEOL JSM-6700F, Japan).

2.3.3. Osteogenesis-related gene and protein expressions. To quantitatively reveal the difference between the mRNA levels of osteogenic markers, gene expressions (such as RUNX2, ALP, BMP-2, OPN, OCN, COL-I) in MSCs on the TLM, SMAT-TLM, and Ca-SMAT-TLM samples were analyzed by real-time polymerase chain reaction (Real-time PCR). After incubation for 3, 7 and 14 days, the total RNA from the different samples was extracted using an RNA kit (Gibco, USA), then 1 μg of RNA from the cells on each sample was reversely transcribed into complementary DNA using a PrimeScripTM RT reagent kit (TaKaRa, Japan). Afterwards, the expression of osteogenesis-related genes was quantified *via* a RT-PCR method, as described in detail in our previous reports.[13,47] Genes and related specific primers are listed in Table 1, and the derived relative expression data were all normalized against glyceraldehyde-3-phosphate dehydrogenase (GAPDH) using the delta Ct method. To explore the variation trend of the

Table 1 The sequences of the specific primer sets

Target	Primer sequences
RUNX2	Forward primer: 5′-TGGTGTTGACGCTGATGGAA-3′
	Reverse primer: 5′-ATACCGCTGGACCACTGTTG-3′
ALP	Forward primer: 5′-CTGAGCGTCCTGTTCTGAGG-3′
	Reverse primer: 5′-GTTCCTGGGTCCCCTTTCTG-3′
BMP-2	Forward primer: 5′-TGAGGATTAGCAGGTCTTTG-3′
	Reverse primer: 5′-CACAACCATGTCCTGATAAT-3′
OPN	Forward primer: 5′-GTGTACCCCACTGAGGATGC-3′
	Reverse primer: 5′-CACGTGTGAGCTGAGGTCTT-3′
OCN	Forward primer: 5′-CTTCGTGTCCAAGAGGGAGC-3′
	Reverse primer: 5′-CAGGGGATCCGGGTAAGGA-3′
COL-I	Forward primer: 5′-TGCAGGGCTCCAATGATGTT-3′
	Reverse primer: 5′-AGGAAGGGCAAACGAGATGG-3′
GAPDH	Forward primer: 5′-ATCAAGTGGGGTGATGCTGG-3′
	Reverse primer: 5′-TACTTCTCGTGGTTCACGCC-3′

intracellular proteins (including ALP activity, OPN, OCN and COL-I) in cells on different samples, after 3, 7, and 14 days of culture, the cell-seeded samples were laid in Triton X-100 (Life Technologies, USA) and subjected to repeated freeze–thaw and shaking cycles. After that, the supernatant was collected and the light absorbance at 450 nm was recorded spectrophotometrically using the respective ELISA assay kits (R&D, USA) to measure the total intracellular ALP activity and protein contents. Three replicates for each group were tested, and the reported value was the average of three independent tests ($n = 3$).

2.3.4. Collagen secretion assay. Sirius red staining was employed to determine the collagen secretion of MSCs on the TLM, SMAT-TLM, and Ca-SMAT-TLM samples. In the quantitative analysis, the cells were seeded on the samples (three replicates in each group) and cultured in an incubator for 3, 7 and 14 days, where at each prescribed time the samples were first fixed with 4% paraformaldehyde and then stained with 0.1% sirius red solution at room temperature overnight. Subsequently, 10% sodium hydroxide solutions were added to the samples to detach the stain, and, after shaking, the optical density of the elution solutions was determined at an absorbance of 540 nm. The obtained data were the average of three independent tests ($n = 3$). To reveal the results more intuitively, images of the secreted collagen of the MSCs were also taken after 7 days of incubation.

2.3.5. Evaluation of ECM mineralization. The osteogenic capacity of MSCs on the TLM, SMAT-TLM, and Ca-SMAT-TLM samples was also evaluated by ECM mineralization using the alizarin red staining method. The detailed procedures were as follows. After the cells were incubated onto the samples (three replicates for each group) for different times (3, 7 and 14 days), where the cell-seeded samples were first fixed with 4% paraformaldehyde for 1 h and then stained with 1% alizarin red for 15 min at 37 °C. After washing the samples three times with distilled water, the stained samples were immersed in 10% cetylpyridinium chloride solutions for 30 min. Finally, the elution solutions were shaken for 15 min and then their optical density was measured at an absorbance of 620 nm. The reported data was the average from three independent tests ($n = 3$). Besides the above quantitative evaluation, images of the ECM mineralization of the MSCs were also taken after 14 days of culture.

2.3.6. Statistical analysis. The obtained data from the above cell experiments were analyzed using the SPSS 14.0 software (USA) and expressed as the mean ± standard deviation (SD) for $n = 3$. Statistically significant differences (p) between the groups were determined by two-way ANOVA followed by a Student–Newman–Keuls *post hoc* test. $p < 0.05$ was considered statistically significant, and $p < 0.01$ was considered highly statistically significant.

2.4. Biomineralization in SBF

The biomineralization capacity of the TLM, SMAT-TLM, and Ca-SMAT-TLM samples was explored by immersing them in SBF for 28 days, was as it has been reported that bone-bonding materials usually form calcium phosphate minerals on their surfaces within 4 weeks.[39,53] SBF was prepared by dissolving the reagent-grade chemicals NaCl, $NaHCO_3$, KCl, $K_2HPO_4 \cdot 3H_2O$, $MgCl_2 \cdot 6H_2O$, $CaCl_2$, and Na_2SO_4 in distilled water, and buffering them at pH 7.4 with tris-hydroxymethyl-aminomethane and HCl at 37 °C, according to work by Kokubo.[53] The ion concentrations (mM) of SBF were 142 Na^+, 5 K^+, 1.5 Mg^{2+}, 2.5 Ca^{2+}, 147.8 Cl^-, 4.2 HCO_3^-, 1 HPO_4^-, and 0.5 SO_4^-, nearly equal to those in human blood plasma.[37] All the samples were immersed in plastic tubes containing 50 mL of SBF at 37 °C, and the SBF was refreshed every two days. At a target time of 28 days, all the immersed samples were taken out of the SBF and washed with distilled water. After being dried in air and sprayed with gold, the morphologies and chemical compositions of the deposited precipitations on the samples were examined by SEM (JSM-6700F) equipped with an EDS probe.

3. Results

3.1. Surface characterization of the samples

The crystal phases of the samples were characterized by XRD, with the results shown in Fig. 1. The TLM sample pattern shows the (110), (200), and (211) reflections located at around $2\theta = 39°$, 56°, and 70°, respectively (Fig. 1(a)), suggesting that it constitutes a sole β-Ti phase.[9,28] After SMAT treatment, the XRD pattern of the SMAT-TLM sample also exhibits diffraction peaks of β-Ti, however, the characteristic peaks are obviously broadened (Fig. 1(b)), which is similar to in our previously reported work,[47] indicating that the grains in this surface layer of the sample are refined. The XRD profile of the Ca-SMAT-TLM sample is quite similar to that of the SMAT-TLM sample, and no shift of the characteristic peaks is observed (Fig. 1(c)), suggesting that the implanted Ca ions rarely enter the β-Ti lattice. Since Ca has been reported to have a very low solubility in titanium,[12] it is reasonable to speculate that the implanted Ca ions tend to form Ca-containing compounds on the β-Ti surface in this work.

The XRD results displayed in Fig. 1, were evidenced by pairs of the OM and TEM results as revealed in Fig. 2. The

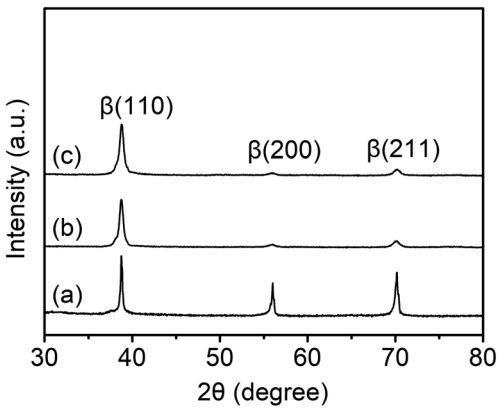

Fig. 1 XRD patterns of the (a) TLM, (b) SMAT-TLM, and (c) Ca-SMAT-TLM samples.

microstructure of the TLM sample features inter-adjacent equiaxed grains, with a measured average grain size of around 170 ± 19 μm (Fig. 2(a)). The surface microstructure of the SMAT-TLM sample is characterized by many randomly distributed nanograins with inconsistent crystallographic orientations (Fig. 2(b)), and the corresponding selected area electron diffraction (SAED) pattern (inset of Fig. 2(b)) exhibits continuous rings attributed to the single β phase, further indicating the generation of very fine β-Ti grains after SMAT. As can be deduced from the dark-field image (Fig. 2(c)), these fine grains normally exhibit an irregular morphology, with an average size of approximately 74 ± 8 nm. Fig. 2(d–f) reveal the surface microstructure of the Ca-SMAT-TLM sample. Similar to Fig. 2(b), abundant grains with nanoscale sizes and irregular shapes are observed in the bright-field image (Fig. 2(d)), and the SAED pattern in the inset of Fig. 2(d) still exhibits continuous rings, but nonetheless, innermost diffraction spots with a *d*-spacing of 0.271–0.273 nm appear, which fit well to the (200) plane of $CaTiO_3$. The dark-field image (Fig. 2(e)), taken on the reflections of $CaTiO_3$(200), reveals that the average size of the formed nanoparticles is around 16 ± 3 nm. The high-resolution TEM (HRTEM) image (Fig. 2(f)) further confirms that these nanoparticles are $CaTiO_3$, which are well crystallized and are bound tightly to the β-Ti substrate.

The surface chemical composition, the elemental depth profile of the Ca-SMAT-TLM sample, and the chemical state of the O in the different samples was analyzed by XPS, with the results shown in Fig. 3. As observed in the survey XPS spectrum (Fig. 3(a)), besides peaks for the O, Ti, C, and Nb elements, Ca peaks were also detected, indicating the successful implantation of Ca ions onto the sample. The high-resolution spectrum

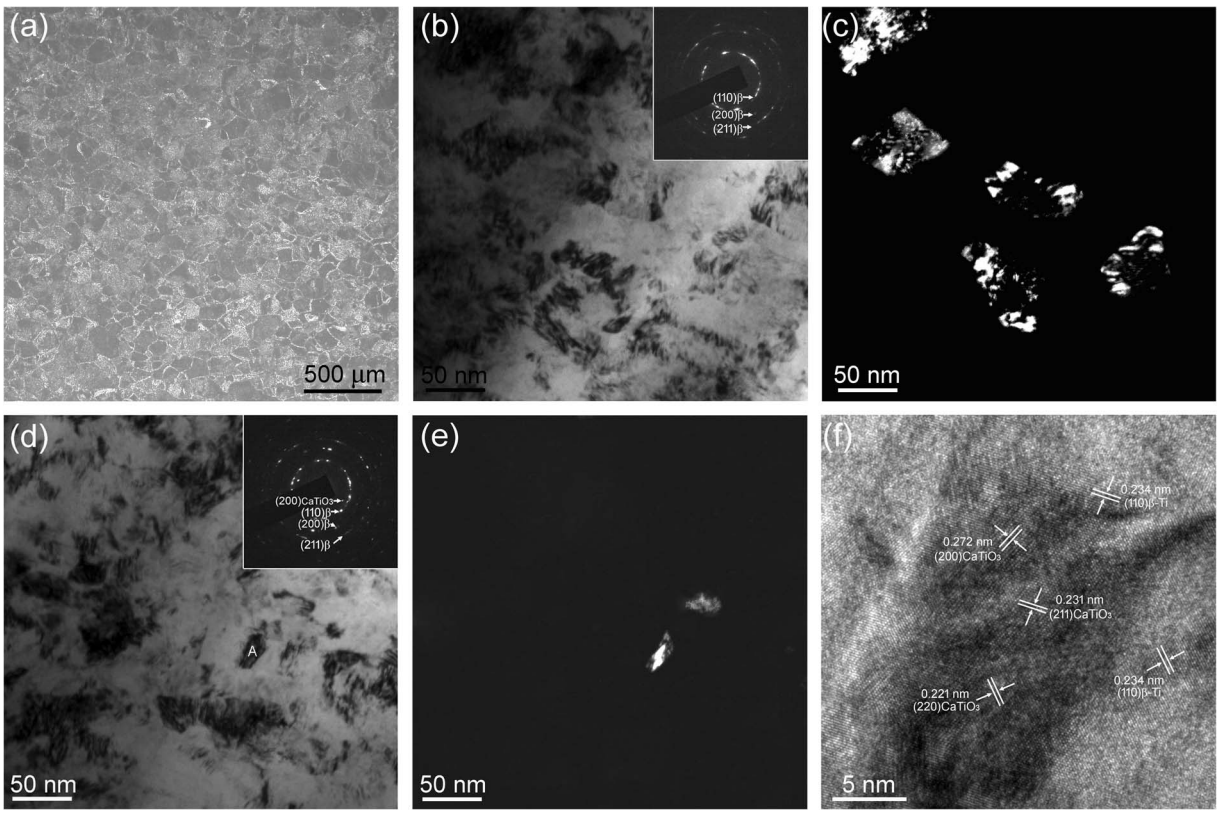

Fig. 2 (a) Optical microscope image of the TLM sample; TEM images taken of the SMAT-TLM sample surface layer: (b) bright-field image, inset is the corresponding SAED pattern, and (c) dark-field image taken of the reflection of the β(110) diffraction ring marked in the inset of (b); TEM images taken from the Ca-SMAT-TLM sample surface layer: (d) bright-field image, inset is the corresponding SAED pattern, (e) dark-field image taken of the reflection of the $CaTiO_3$(200) diffraction spots marked in the inset of (d) and (f) HRTEM image of a typical $CaTiO_3$ particle marked in (d) with a letter A.

of Ca 2p (Fig. 3(b)) exhibits double peaks at a binding energy of around 346.5 eV (2p 3/2) and 349.9 eV (2p 1/2), suggesting the formation of $CaTiO_3$,[13,38] in accordance with the TEM results. The XPS depth profiles of O, Ti, Nb, and Ca are revealed in Fig. 3(c). On the outermost surface of the sample, O exhibits the highest atomic concentration while Ti and Nb exhibit the lowest concentrations. However, the implanted Ca depth profile displays Gaussian-like distributions, it shows a maximum implantation depth of 128 nm and a peak concentration of 21.9 at% at a distance of around 14 nm from the topmost surface. To further explore the effect of the treatment process on the variation of the surface oxide layer, the chemical state of the O element on different samples was characterized and the result are shown in Fig. 3(d). As seen from this figure, the original O 1s spectra of the different samples can be deconvoluted into three Gaussian component peaks at 530.1, 531.3, and 532.8 eV, which correspond to O^{2-}, physisorbed water and Ti–OH groups, respectively.[38,54] The fitted percentage areas of the deconvoluted peaks are shown in Table 2, from which it is indicated that SMAT and the subsequent Ca-ion implantation decrease the ratio of physisorbed water and simultaneously increase the content of Ti–OH groups in the surface layer of the TLM alloy.

SEM images of the morphology and EDS two-dimensional mapping of Ca, O, Ti, and Nb of the Ca-SMAT-TLM sample are shown in Fig. 4. SEM analysis reveals that the Ca-SMAT-TLM sample mainly features many craters with sizes of around hundreds to thousands of nanometers. The merged elemental image shows that each element is generally evenly distributed throughout the surface. However, the implanted Ca element was observed to be distributed highly in correlation with the distribution of Ti and O, indicating that Ca tends to combine with Ti and O to form calcium titanium compounds after ion implantation, further confirming the TEM and XPS analysis results.

Table 2 Area percentage of the peaks at different binding energies

	Different peak area percentage of O 1s (%)		
Sample	530.1 eV	531.3 eV	532.8 eV
TLM	60.9	29.5	9.6
SMAT-TLM	63.7	24.6	11.7
Ca-SMAT-TLM	64.5	18.1	17.4

The surface topography of the TLM, SMAT-TLM, and Ca-SMAT-TLM samples was measured by AFM, as shown in Fig. 5(a–c). The TLM sample exhibits a relatively flat and smooth surface due to its pre-polishing treatment (Fig. 5(a)), while the SMAT process creates numbers of overlapping indentations and craters on the SMAT-TLM sample (Fig. 5(b)), and the subsequent Ca ion implantation does not induce significant alteration of the SMAT-generated surface topographic features

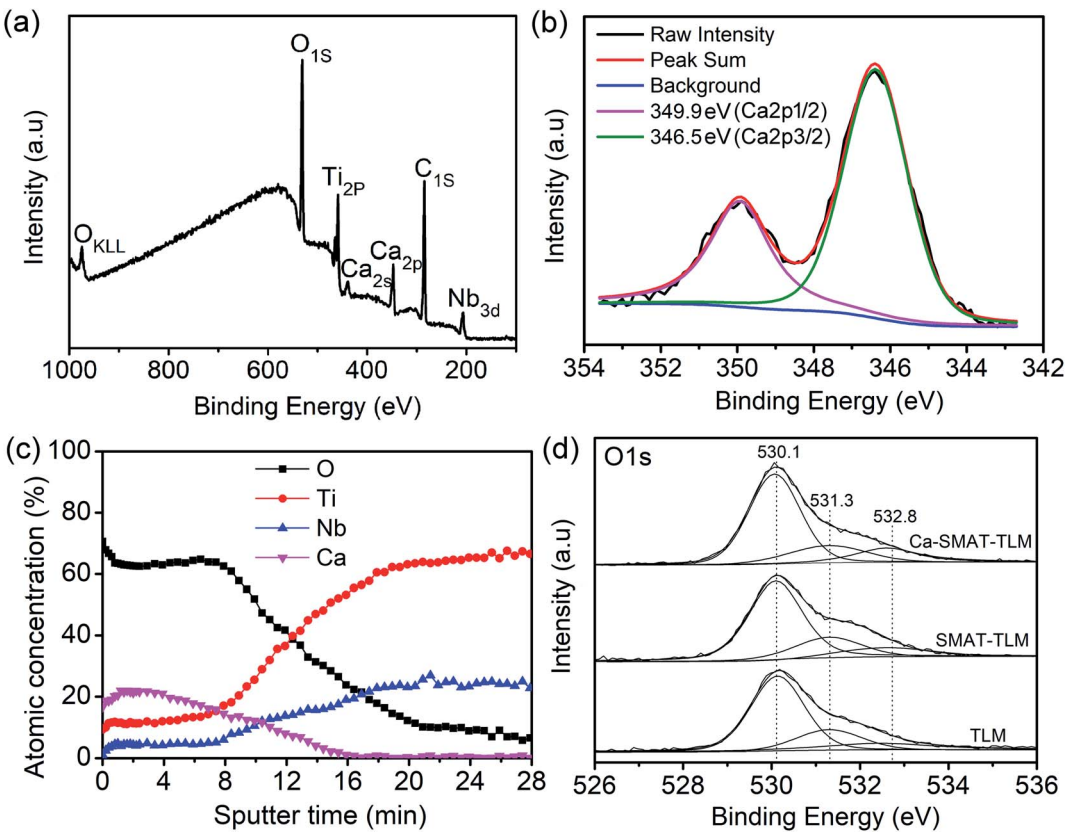

Fig. 3 (a) Wide-scan survey spectra, (b) high-resolution Ca 2p XPS spectra, and (c) depth profiles acquired from the Ca-SMAT-TLM sample; (d) O 1s XPS spectra of the TLM, SMAT-TLM, and Ca-SMAT-TLM sample surfaces.

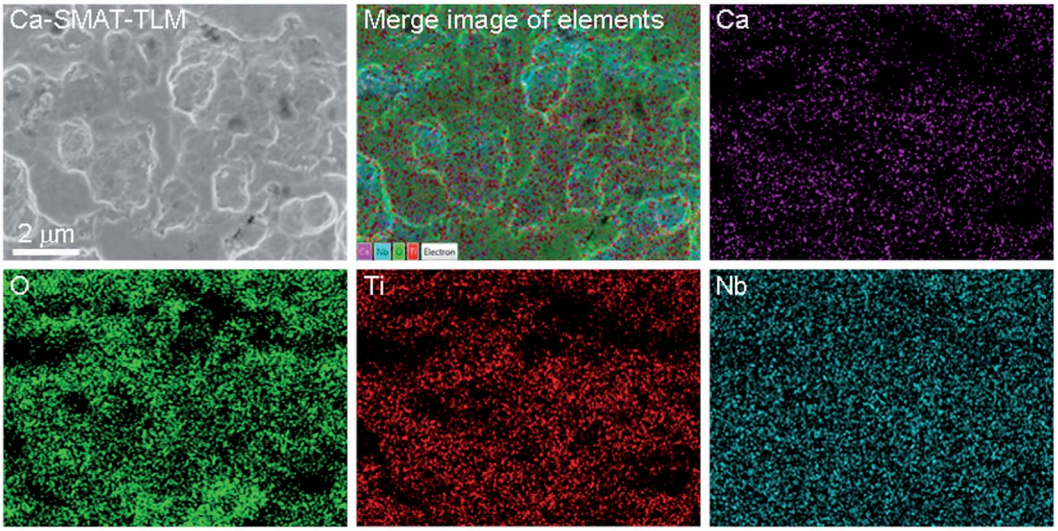

Fig. 4 SEM surface morphological image and EDS distribution of the Ca, O, Ti and Nb of the Ca-SMAT-TLM sample.

(Fig. 5(c)). The above variation trend was further confirmed by the measured surface roughness parameters of the different samples, as presented in Table 3. It can be clearly seen that the SMAT-TLM sample exhibits much greater surface roughness compared to the TLM sample, with a similar surface roughness to that of the Ca-SMAT-TLM sample. Fig. 5(d) presents the static water contact angle values on the various samples. The TLM sample displays a contact angle of 70.8 ± 3.5°, and the SMAT-

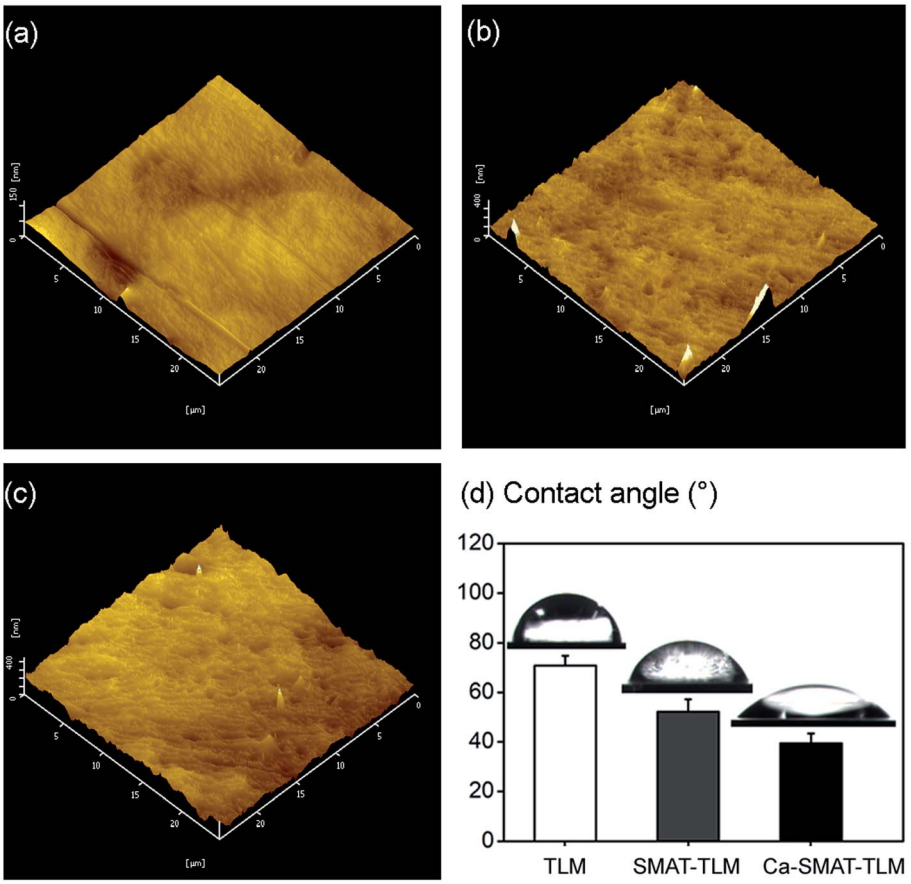

Fig. 5 AFM images of the (a) TLM, (b) SMAT-TLM, and (c) Ca-SMAT-TLM samples; (d) histogram of the static water contact angles of the different samples.

Table 3 Roughness measured by AFM analysis of TLM, SMAT-TLM, and Ca-SMAT-TLM sample surfaces, data are presented as mean ± SD ($n = 3$)

Roughness (nm)	TLM	SMAT-TLM	Ca-SMAT-TLM
Ra	16.1 ± 1.5	47.6 ± 4.8	45.9 ± 3.2
Rq	26.2 ± 2.4	84.5 ± 6.7	82.8 ± 7.4
Rz	71.4 ± 4.6	236.4 ± 11.3	229.8 ± 12.1

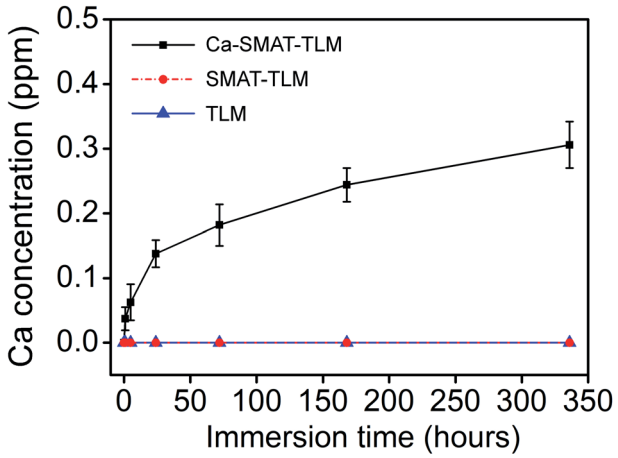

Fig. 6 Cumulative release profile of Ca from various samples into α-MEM containing 10% FBS after immersion for different times.

TLM sample shows a contact angle of 52.2 ± 4.7°, while the contact angle of the Ca-SMAT-TLM sample is 39.4 ± 3.8°. Previous studies have reported that the Ti–OH groups on titanium are very helpful for improving surface hydrophilic properties,[13,54] where the Ti–OH contents in the O 1s XPS spectra of the TLM, SMAT-TLM, and Ca-SMAT-TLM sample in this work are 9.6%, 11.7%, and 17.4% respectively (Table 2). Hence, the surface wettability of the TLM alloy is in the order of Ca-SMAT-TLM > SMAT-TLM > TLM.

Fig. 6 depicts the ICP-AES results of Ca ions leached from the different samples. As can be observed, during the test period, no Ca ions were detected for the TLM and SMAT-TLM samples, while the Ca ions were found to be sustainably released from the Ca-SMAT-TLM sample into the cell culture medium, with the measured Ca concentration reaching 0.31 ppm after the longest immersion time of 14 days.

The protein adsorption behavior of the different samples was measured after their incubation in the cell culture medium for 1, 5, and 24 h, as revealed in Fig. 7. The results presented in Fig. 7(a) show that the total amounts of adsorbed proteins on each sample increased with a prolonging of the incubation time, with the increase mainly occurring from 1 to 5 h. In addition, at each time point, the amount of adsorbed total proteins was found to be the greatest on the Ca-SMAT-TLM sample, with that of the SMAT-TLM sample greater than on the TLM sample. Similar results were also obtained for the specific proteins Ln, Fn, and Vn, with the difference being in the

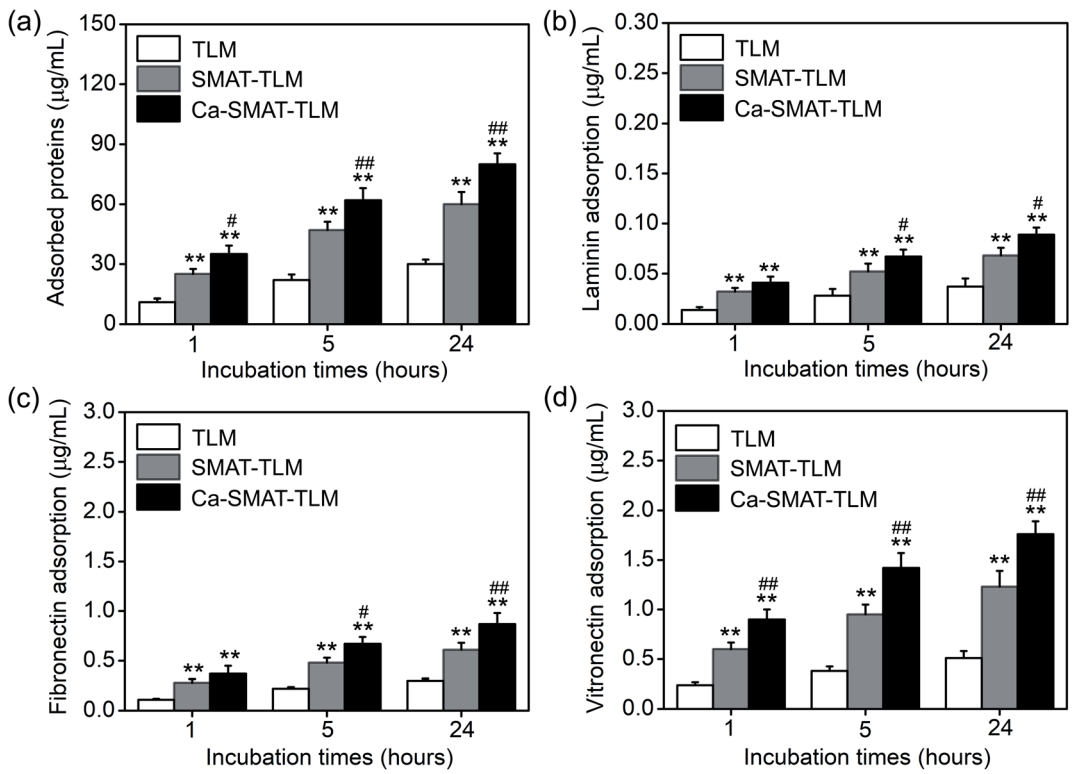

Fig. 7 Adsorption of (a) total protein, (b) Ln, (c) Fn, and (d) Vn onto different samples after 1, 5 and 24 h of incubation in α-MEM containing 10% FBS. Data are presented as the mean ± s.d. (standard deviation), $n = 3$. **$p < 0.01$ compared with the TLM sample, #$p < 0.05$ and ##$p < 0.01$ compared with the SMAT-TLM sample.

unequal levels of adsorbed protein contents at each time on each sample (Fig. 7(b–d)). At each incubation time, the amounts of Ln, Fn, and Vn, as well as total proteins adsorbed onto the samples, follow the trend of Ca-SMAT-TLM > SMAT-TLM > TLM.

3.2. Cell response studies

The adhesion and proliferation conditions of MSCs on the samples were characterized by determining the number of viable cells using the CCK-8 assay, and the acquired results are shown in Fig. 8. At incubation time of 1, 5 and 24 h, compared to the TLM sample, the SMAT-TLM sample remarkably increased the adherent cell number while the Ca-SMAT-TLM sample exhibited the highest number (Fig. 8(a)). As time progressed, the cells on the different samples all proliferated. Although the cell proliferation was observed to be greatly accelerated on the SMAT-TLM sample, the acceleration was more pronounced on the Ca-SMAT-TLM sample compared to on the TLM sample (Fig. 8(b)). The statistical difference between the SMAT-TLM and Ca-SMAT-TLM samples becomes more significant ($\#p < 0.05$ for 1, 5, 24 h and $\#\#p < 0.01$ for 3, 7, 14 days), implying that the gradual release of Ca ions was beneficial to the cell proliferation of the MSCs. To further explore the effect of the different surfaces on the MSC adhesion, the typical individual cell shape after 5 h of cultivation was observed under SEM. As seen from Fig. 8(c), the cells on the TLM sample show a spherical shape, those on the SMAT-TLM sample present a polygonal shape, and a more flattened morphology is observed when cells adhere to the Ca-SMAT-TLM sample. These results indicate that the implantation of Ca ions onto the SMAT-treated TLM alloy provides a very comfortable surface for MSCs on which to adhere and grow.

The osteogenic differentiation ability of MSCs is critical to the successful osteointegration of an implant,[27,45] therefore the osteoblastic differentiation capacity of MSCs on the samples was evaluated by the determination of the mRNA expression levels of several osteogenesis-related gene markers. The obtained results are shown in Fig. 9, from which it can be seen that all the samples promote osteogenic gene expression in the MSCs to varying extents. For RUNX2, BMP-2, OCN and COL-I markers, the mRNA expression levels of the cells on each sample sustainably increased with an incubation time of up to 14 days (Fig. 9(a, c, e and f)), however, at 7 days, the expression peak of ALP (Fig. 9(b)) and OPN (Fig. 9(d)) was observed for the Ca-SMAT-TLM sample, suggesting the more rapid osteodifferentiation rate on its surface.[55] Overall, the MSCs grown on the SMAT-TLM sample reveal statistically significantly higher ($*p < 0.05$ and $**p < 0.01$) mRNA expressions of the osteogenesis-related gene markers (RUNX2, ALP, BMP-2, OPN, OCN and COL-I) than those cultured on the TLM sample, nevertheless, the Ca-SMAT-TLM sample exhibits a stronger positive effect of boosting the osteogenic differentiation of MSCs than the other two group samples. The above trend was further proved by the protein expressions of MSCs, as depicted in Fig. 10(a). As can be observed, the measured intracellular ALP

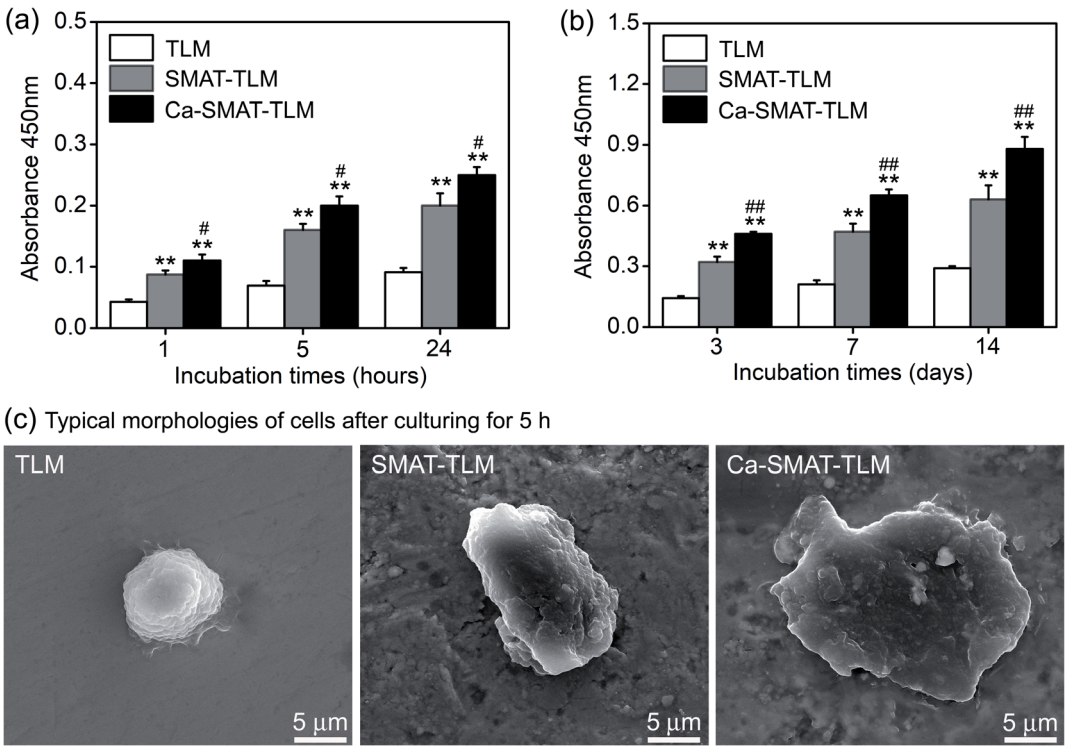

Fig. 8 (a) MSC adhesion measured by CCK-8 after 1, 5, and 24 h of culture, (b) MSC proliferation measured by CCK-8 after 3, 7, and 14 days of culture, (c) SEM images of the MSCs after culturing for 5 h on different samples. $**p < 0.01$ compared with the TLM sample, $\#p < 0.05$ and $\#\#p < 0.01$ compared with the SMAT-TLM sample.

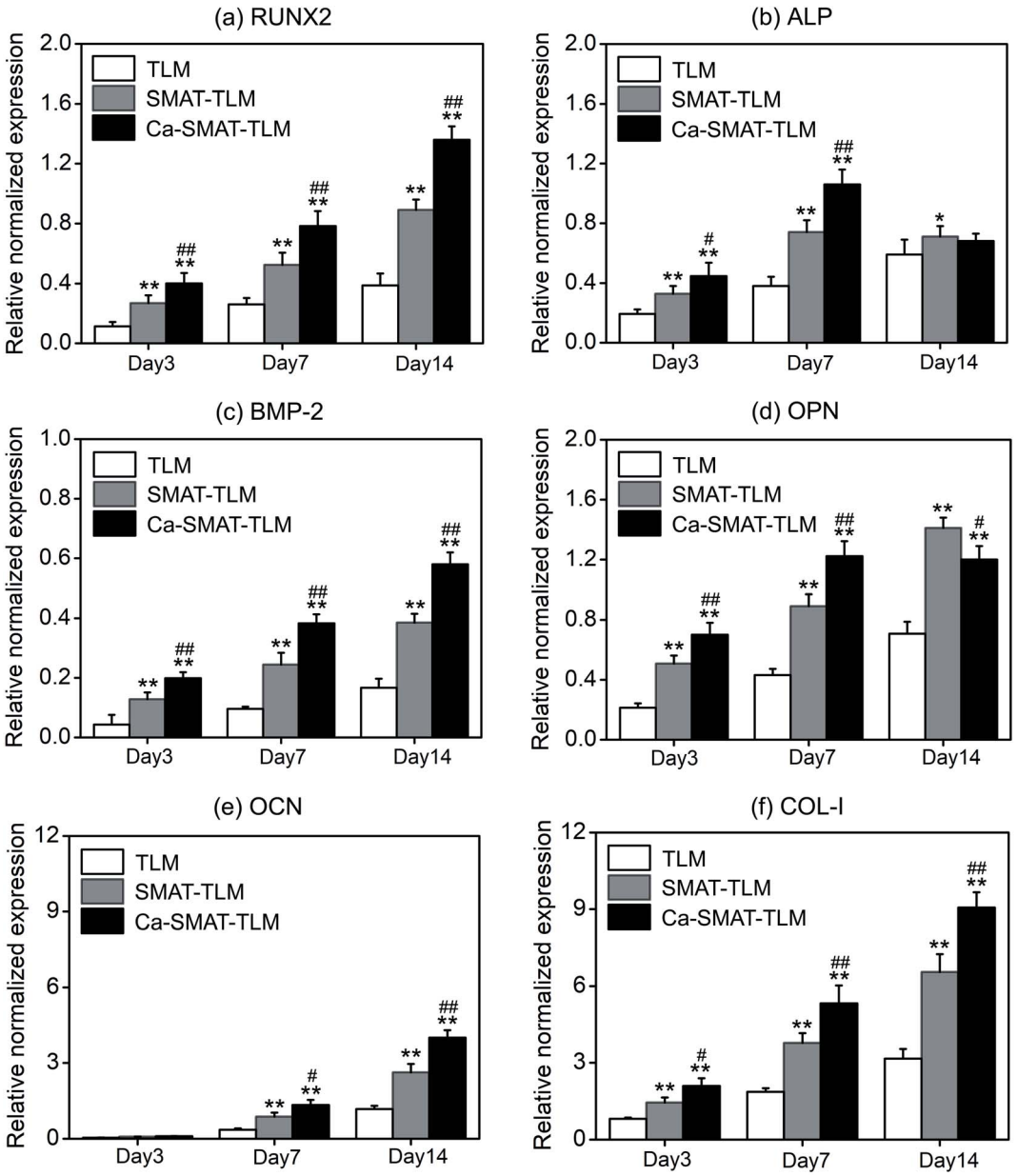

Fig. 9 Osteogenesis-related gene expressions of the MSCs after 3, 7 and 14 days of culture on various samples. *p < 0.05 and **p < 0.01 compared with the TLM sample, #p < 0.05 and ##p < 0.01 compared with the SMAT-TLM sample.

activity and specific protein (OPN, OCN and COL-I) contents on the samples after incubation for different times (3, 7 and 14 days) vary analogously to the corresponding gene expression, as the protein is a downstream product of the gene.[13,55]

The quantitatively determined collagen secretion of MSCs on different samples is shown in Fig. 10(b). The amount of the collagen secreted by the cells onto each sample was observed to increase prolonged culture time from 3 to 14 days. In particular, at each target time, the collagen amount was perceived to be greater on the SMAT-TLM sample, and much greater on the Ca-SMAT-TLM sample compared to that on the TLM sample. Furthermore, the ECM mineralization capacity of MSCs on the various samples was also assessed using the sirius red staining method after incubation for 3, 7 and 14 days. Although all of the samples revealed an affirmative effect on the promotion of mineralization with an extension in the time, the mineralization level on the Ca-SMAT-TLM sample was significantly higher than that on the TLM and SMAT-TLM samples (especially for the TLM sample) at all time intervals (Fig. 10(c)). Staining images provide more visual evidence to support the above fact, where it can be seen from Fig. 11 that much denser collagen deposition (Fig. 11(a)) and ECM mineralization (Fig. 11(b)) occurred on the Ca-SMAT-TLM sample as compared with the TLM and SMAT-TLM samples (especially the TLM sample) after culturing for 7 and 14 days, respectively. The aforementioned results combinedly show that the collagen secretion and ECM

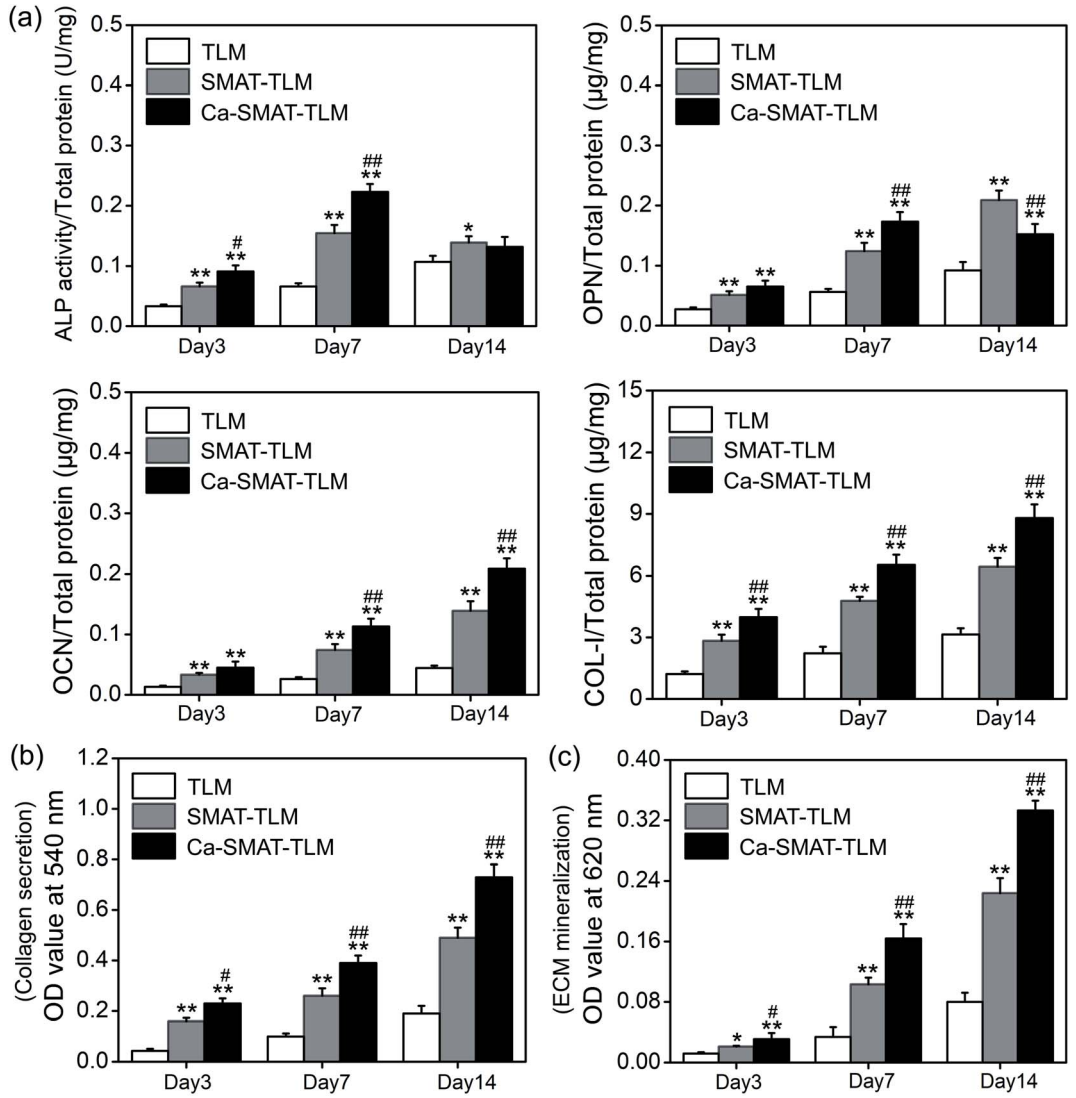

Fig. 10 (a) ALP activity, contents of OPN, OCN and COL-I protein levels, (b) collagen secretion, and (c) ECM mineralization after 3, 7 and 14 days of MSC incubation on the different samples. *$p < 0.05$ and **$p < 0.01$ compared with the TLM sample, #$p < 0.05$ and ##$p < 0.01$ compared with the SMAT-TLM sample.

mineralization of the MSCs are more active on the surface with the introduction of Ca ions.

3.3. Biomineralization capacity of the samples

To compare their biomineralization ability, the TLM, SMAT-TLM, and Ca-SMAT-TLM samples were immersed in SBF for 28 days. From Fig. 12, it can be seen that after SBF incubation, no deposits were observed on the TLM (Fig. 12(a)) and SMAT-TLM samples (Fig. 12(b)). However, island-like layers constituted by many ball-like deposits were found to cover the Ca-SMAT-TLM sample (Fig. 12(c)), and the EDS detection of a typical deposit (marked in Fig. 12(c) with a letter B) further confirmed that the newly formed layers were Ca- and P-containing minerals with a Ca/P ratio of around 1.58 (Fig. 12(d)). These results suggest that the Ca-SMAT-TLM sample possesses superior biomineralization capacity compared to the TLM and SMAT-TLM samples in this study.

4. Discussion

Although titanium implants are most extensively used in bone anchoring systems, the stress-shielding effect induced by the significant difference of the elastic modulus between the implant and the host tissue becomes an obstacle to impeding their wider clinical use.[1,14] In the present work, the TLM alloy with a modulus of approximately 69 GPa[46] was selected as the substrate, which is close to the modulus of cortical bone (about 15–30 GPa[3]), therefore meaning that it could be efficient in reducing the risks of osteanabrosis and bone resorption due to stress shielding.

Aside from the elastic modulus, limited osseointegration of the implant and bone is another issue that hinders the broader application of Ti-based alloy in the clinic.[4,5,31] It has been acknowledged that refining grains by means of equal channel angular pressing (ECAP)[56,57] and high-pressure torsion (HPT)[58,59]

Fig. 11 (a) Sirius red staining pictures of collagen secretion after 7 days of MSCs culturing on the different samples, and (b) pictures of ECM mineralization determined by alizarin red staining after 14 days of MSCs culturing on the samples.

could improve cell–material interactions, thus boosting the osseointegration of Ti-based alloys. However, the elastic modulus is also elevated after these bulk-nanostructuring treatments, which in turn aggravates the mismatch in the moduli of the implant and bone. In this regard, the SMAT method, which refines the grains in the surface layer of Ti-based

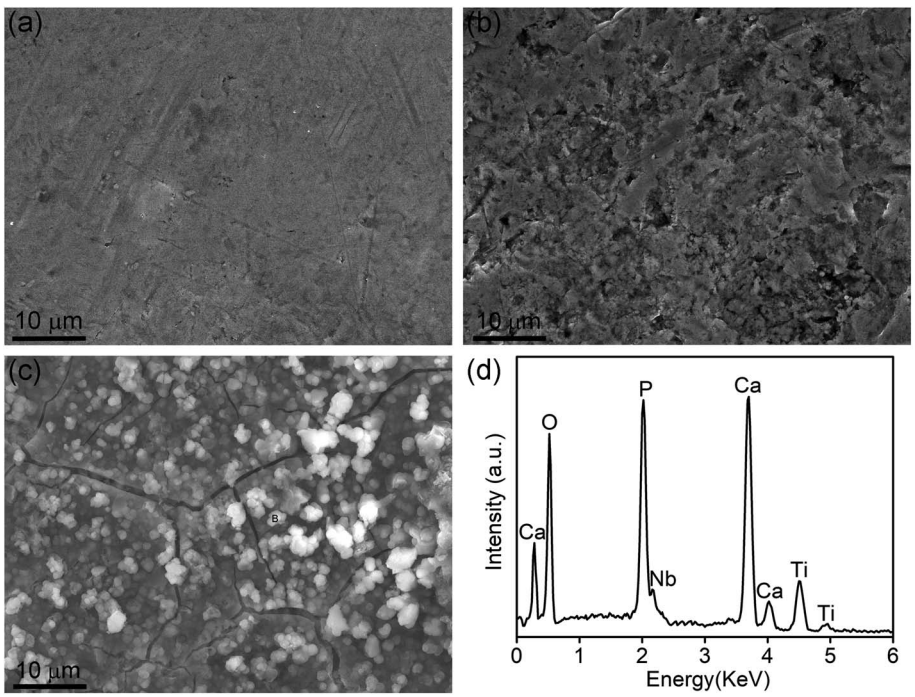

Fig. 12 SEM images of mineral deposition on the (a) TLM, (b) SMAT-TLM, and (c) Ca-SMAT-TLM samples after a soaking period of 28 days in SBF; (d) the EDS spectrum of the point marked in (c) with a letter B.

alloys to endow the implants with rapid osseointegration while preserving the mechanical properties of the substrates, reveals good potential for use in the development of new-generation bone-associated substitute materials.

In this study, the SMAT technique was adopted to treat a TLM alloy, and the modified surface with a much smaller grain size, much larger roughness and better hydrophilicity was verified to enhance MSC adhesion, proliferation and osteogenic functions. It has been reported that the first step for a biomaterial after implantation into body is protein adsorption, where the adsorbed protein layer of the recruited cells senses the foreign surface.[23] The SMAT-TLM sample possesses a much larger fraction of grain boundaries on its surface compared to the TLM sample (Fig. 2(a–c)), which facilitates the adsorption of more protein on its surface (Fig. 7(a)) due to increased surface energy. Additionally, contact angle measurements proved that the SMAT-TLM sample exhibits much better hydrophilic properties than the TLM sample (Fig. 5(d)), which is reported to be capable of keeping adsorbed proteins on its surface in a more desirable conformation.[9] Previously, Luo *et al.*[10] confirmed that the nanostructured titanium with a more hydrophilic surface increases the amount of adsorbed protein, thus promoting the adhesion of MG63 cells. Huo *et al.*[20] reported that SFT-derived nanograined Ti6Al4V with a more hydrophilic surface promoted the adsorption of RGD (arginine–glycine–aspartic acid)-containing anchoring proteins in a more active conformation, thereby improving osteoblastic adhesion. The SMAT-TLM sample herein adsorbed more RGD-containing anchoring proteins such as Ln, Fn and Vn (Fig. 7(b–d)) on its surface compared to the TLM sample, which created a comfortable environment to improve the MSC adhesion. Besides the above-mentioned surface grain structure and hydrophilicity, the surface roughness might be another reason why the TLM alloy exhibited better cell adhesion after SMAT treatment. The positive effect of surface roughness at the micro/nanoscale on the adhesion of osteoblasts has been proved. Sun *et al.*[22] adopted the SMAT process to treat pure titanium and found that the obtained microrough surface promoted the attachment and viability of co-cultured MG63 cells. As reported by Bagherifard *et al.*, the higher surface density of nano-irregularities provided by nano-rough 316L stainless steel favorably contributed toward regulating the interaction of material with cells.[51,52] The SMAT-TLM sample exhibits a much higher surface roughness (Table 3), which would have greater contact with the MSCs than the smooth TLM sample and thus result in enhanced MSC adhesion on its surface.

When cells come into contact with implanted materials, adhesion is the first event, which in turn determines the subsequent cellular behavior, such as cell proliferation, differentiation and mineralization.[27,47,60] After 3, 7 and 14 days of culture, CCK-8 assay (Fig. 8(b)) revealed that the MSCs adhered to the SMAT-TLM sample, presenting higher proliferation compared to the TLM sample, suggesting that the SMAT-achieved nanograined surface was helpful for the proliferation of MSCs. Barring cell adhesion and proliferation, cell differentiation is a very important evaluation point for materials because it directly influences bone tissue repair. MSCs are multi-lineage potential cells that self-renew and differentiate into every type of cell, such as adipogenic cells, endothelial cells, chondrocytes and osteoblasts, therefore their differentiation capacity toward osteoblastic lineage is essential for bone regeneration.[34] The results of RT-PCR analysis in this work indicate that the SMAT-TLM sample accelerates osteogenic differentiation of MSCs. At each culture time point, MSCs growing on the SMAT-TLM sample displayed stronger expression of mRNA levels of key osteogenic genes: RUNX2, ALP, BMP-2, OPN, OCN and COL-I as compared to the TLM sample. RUNX2 and ALP are early markers of the osteogenesis of osteoblasts,[27,60] OPN and OCN (mature osteoblast markers) are two kinds of noncollagenous matrix proteins that play important roles in bone mineralization.[9] BMP-2 and Type I collagen are of significance for the development and maintenance of the phenotype of osteoblasts.[33,47,61] With the up-regulation of these osteo-related gene expressions (Fig. 9(a–f)), the respective protein contents in the cells were also observed to be promoted (Fig. 10(a)), thus causing more proteins such as COL-I to secrete into the ECM (Fig. 10(b) and Fig. 11(a)), ultimately leading to the acceleration of ECM mineralization, as depicted in Fig. 10(c) and Fig. 11(b).

The aforementioned SMAT-TLM sample was verified to be capable of enhancing the osteogenesis of MSCs. From our study, it is interesting to note that the subsequent implantation of Ca ions onto the SMAT-TLM sample further promoted the adhesion, proliferation, and osteogenic properties (including osteogenic differentiation and ECM mineralization) of the MSCs. The subsequent Ca-ion implantation had little impact on the roughness and topography of the SMAT-TLM sample, accordingly, the surface chemistry provided by the formed Ca-containing compound and the increased hydrophilicity after ion implantation were responsible for the improved osteogenetic behavior of the MSCs. It was reported that the implantation of Ca ions onto pure titanium could alter the surface chemistry, resulting in changes in surface energy and hydrophilicity, and through these changes the Ca-ion implanted samples adsorbed and/or desorbed different ions and biomolecules from the near-surface environment, consequently mediating the cellular response.[15] Ko *et al.* also suggested that there was direct electro-chemical bonding between the Ca ions and proteins, which benefited the attachment of MC3T3-E1 cells.[33] The subsequent ion implantation in this work imparts the Ca-SMAT-TLM sample with superior hydrophilicity (Fig. 5(d)) and protein adsorption ability (Fig. 7) to the SMAT-TLM sample, hence promoting the adhesion of MSCs (Fig. 8). In addition, it has been well documented that extracellular Ca is a critical regulator of cell behavior and plays an important role in modulating cell proliferation and differentiation.[14,42]

A previous study revealed that extracellular Ca ions promote the proliferation of BM-hMSCs at the initial stage, and then induce osteogenesis of cells and the formation of mineral nodules at a later stage through the MAPK signaling pathway.[62] Lee *et al.* explored Ca^{2+} released from a bone resorption surface and found that extracellular Ca^{2+} is a key factor in the expression of the MSC population in bone remodeling sites, activating cell proliferation and migration.[63] Barradas *et al.*[64] reported that

the released Ca^{2+} triggers the signaling pathway not only using a calcium-sensing receptor but also using type L-voltage-gated channels to regulate the osteogenesis and proliferation of hMSCs. In this study, the Ca-SMAT-TLM sample releases a large amount of Ca ions into the cell culture medium in a time-dependent manner (Fig. 6), which is considered to contribute toward the enhancement of the expression of osteogenic genes (Fig. 9) and encoding characteristic proteins (Fig. 10(a)) during osteogenic differentiation. Moreover, it is worth noting that lower ALP and OPN gene/protein expressions were observed on the Ca-SMAT-TLM sample after day 7. An ALP marker was recognized with peak mRNA expression and activity levels proclaiming the maturation of osteoblasts and then the levels decreased at the onset of mineralization.[9,47] OPN is involved in the onset of ECM mineralization, with the peak level indicating the secreted ECM maturation.[60,65] The obtained results collectively suggest that the subsequent implantation of Ca ions onto the SMAT-processed sample positively influenced the differentiation of MSCs *in vitro* toward the osteogenic lineage, not only by progressing the cells into a mature phenotype but also by accelerating ECM mineralization at an earlier time. Overall, the potential mechanism for the Ca-SMAT-TLM sample regulating the behavior of MSCs is displayed in Fig. 13, which can be summarized as follows. Firstly, the increased nanoscale surface roughness combined with the refined grain structure might provide more optimal sites for cells to adhere, which is beneficial for the initial adhesion of the MSCs. Secondly, with the improved surface hydrophilicity, the sample could adsorb more RGD-contained anchoring proteins such as Ln, Fn and Vn necessary for cell adhesion and create a favorable osteogenic microenvironment for the subsequent cell proliferation, osteo-differentiation and ECM mineralization of the MSCs. Thirdly, the gradual release of Ca^{2+} from the surface layer could trigger different signaling pathways to further promote the osteogenic function of MSCs.

Besides the investigation of the osteogenic activity of MSCs on the TLM, SMAT-TLM, and Ca-SMAT-TLM samples, in the present work, the biomineralization properties of different samples were also assessed *via* SBF soaking experiments, and the Ca-SMAT-TLM sample was found to be able to significantly boost the deposition of Ca and P containing minerals on its surface. The reason for this is as follows. As deduced from Fig. 3(d) and Table 2, the Ca-SMAT-TLM sample possesses a much higher ratio of Ti–OH groups on its surface as compared to the TLM and SMAT-TLM samples, where the Ti–OH groups have been reported to be negatively charged and tend to selectively combine with the positively charged Ca^{2+} ions in the SBF to form a Ca-rich vicinity.[38,54] As the calcium ions accumulate, the surface gradually appears to be positively charged, thus combining with anion radicals such as PO_4^{3-} ions in the SBF to form Ca–P containing minerals. In this work, using a two-step approach of combining the SMAT and Ca-ion implantation process endowed the Ti-based alloy with advanced osteogenic and biomineralization properties, providing a promising candidate for the design and fabrication of Ti-based implants in the future.

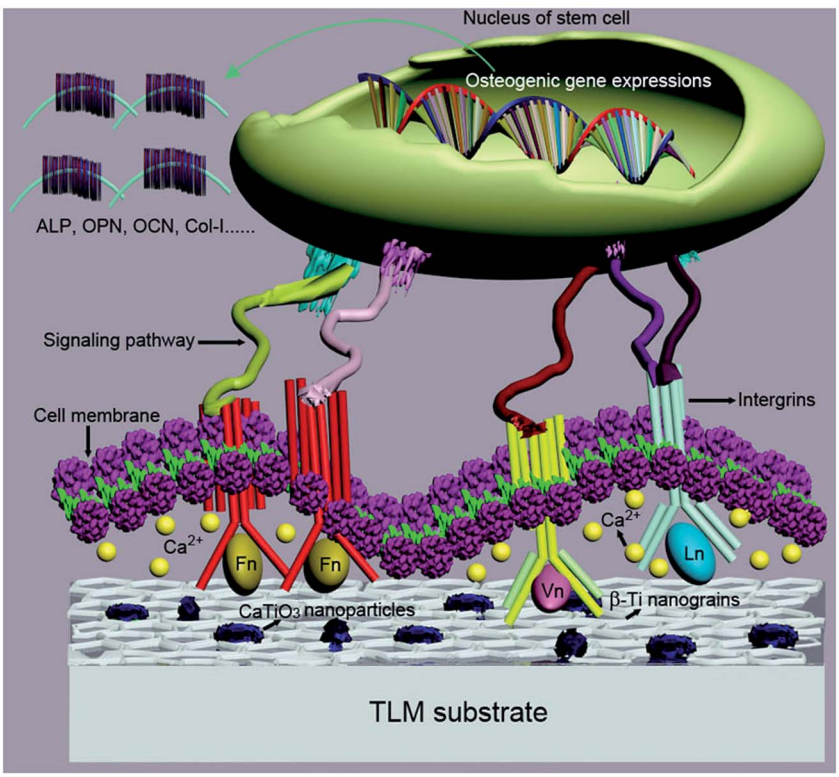

Fig. 13 Possible mechanism of how the Ca-SMAT-TLM sample regulates the osteogenetic behavior of the MSCs.

5. Conclusions

A nanocrystalline surface with an average grain size of 74 ± 8 nm was fabricated on the SMAT-TLM sample. The SMAT-TLM sample exhibited much higher surface roughness and better hydrophilicity compared to the untreated TLM sample. The subsequent Ca-ion implantation did not change the surface roughness and topography obviously, while further enhancing the surface wettability of the SMAT-TLM sample. *In vitro* cell experiments indicated that the SMAT-TLM sample remarkably promoted the cell adhesion, proliferation, osteogenic differentiation, collagen secretion and ECM mineralization of MSCs compared to the TLM sample, while the Ca-SMAT-TLM sample was observed to be capable of further enhancing MSC adhesion and osteogenic functions. A potential mechanism was proposed wherein both the adsorption of more RGD-containing anchoring proteins (such as Ln, Fn and Vn) and the increase in extracellular Ca concentrations contributed toward the enhanced osteogenic activity of MSCs on the Ca-SMAT-TLM sample. Besides the improved osteogenic properties, the Ca-SMAT-TLM sample was also observed to significantly boost the deposition of Ca and P containing minerals on its surface, which was associated with the generation of more Ti–OH groups on the sample after ion implantation. Our study suggests that using the two-step method of combined SMAT and Ca-ion implantation surface treatments endowed the TLM alloy with outstanding osteogenic and biomineralization properties, providing new insights for the biofunctionalization of Ti-based implants to be utilized in the clinic.

Author contributions

Run Huang: conceptualization, resource, funding acquisition, project administration, supervision, writing–review & editing. Yufei Hao: writing-original draft, investigation. Yusong Pan: methodology, resource. Chengling Pan: visualization. Xiaolong Tang: formal analysis. Lei Huang: data curation. Chao Du: investigation. Rui Yue: resource. Diansheng Cui: validation.

Conflicts of interest

There are no conflicts of interest to declare.

Acknowledgements

We appreciate the Natural Science Research Project of Anhui Universities (Grant numbers KJ2020A0304 and KJ2019A0127), the Research Foundation of the Institute of Environment-friendly Materials and Occupational Health of Anhui University of Science and Technology (Wuhu) (Grant numbers ALW2021YF07 and ALW2020YF11), the National Natural Science Foundation of China (Grant numbers 81501598, 81872017 and 82071862), the Primary Research & Development of Anhui Province (Grant number 1804a09020076) and the Postdoctoral Foundation of Anhui Province (Grant number 2017B211) for financially supporting this work. The authors also appreciate Mr Mingce Huang for his generous help in improving the readability of this text.

References

1 M. Geetha, A. K. Singh, R. Asokamani and A. K. Gogia, Ti based biomaterials, the ultimate choice for orthopaedic implants-A review, *Prog. Mater. Sci.*, 2009, **54**, 397–425.
2 T. Hanawa, Titanium-tissue interface reaction and its control with surface treatment, *Front. Bioeng. Biotechnol.*, 2019, **7**, 170.
3 M. Kaur and K. Singh, Review on titanium and titanium based alloys as biomaterials for orthopaedic applications, *Mater. Sci. Eng., C*, 2019, **102**, 844–862.
4 M. Q. Cheng, Y. Q. Qiao, Q. Wang, G. D. Jin, H. Qin, Y. C. Zhao, X. C. Peng, X. L. Zhang and X. Y. Liu, Calcium plasma implanted titanium surface with hierarchical microstructure for improving the bone formation, *ACS Appl. Mater. Interfaces*, 2015, **7**, 13053–13061.
5 J. H. Zhou, B. Li, Y. Han and L. Z. Zhao, The osteogenic capacity of biomimetic hierarchical micropore/nanorod-patterned Sr-HA coatings with different interrod spacings, *Nanomed-Nanotechnol.*, 2016, **12**, 1161–1173.
6 P. C. Wong, S. M. Song, P. H. Tsai, Y. Y. Nien, J. S. C. Jang, C. K. Cheng and C. H. Chen, Relationship between the surface roughness of biodegradable Mg-based bulk metallic glass and the osteogenetic ability of MG63 osteoblast-like cells, *Materials*, 2020, **13**, 1188.
7 M. Suarez, S. Perez-lopez, C. Prado, A. Fernandez, J. S. Moya, R. Torrecillas and L. A. Diaz, Influence of roughness on initial *in vitro* response of cells to Al_2O_3/Ce-TZP nanocomposite, *Journal of Asian Ceramic Societies*, 2021, **9**, 131–141.
8 B. Abar, C. Kelly, A. Pham, N. Allen, H. Barber, A. Kelly, A. J. Mirando, M. J. Hilton, K. Gall and S. B. Adams, Effect of surface topography on *in vitro* osteoblast function and mechanical performance of 3D printed titanium, *J. Biomed. Mater. Res.*, 2021, **109**, 1792–1802.
9 R. Huang, S. M. Lu and Y. Han, Role of grain size in the regulation of osteoblast response to Ti-25Nb-3Mo-3Zr-2Sn alloy, *Colloids Surf., B*, 2013, **111**, 232–241.
10 X. Luo, C. Liang, N. Li, Y. H. Zhu, N. J. Cao, J. Wang, K. D. Liu, H. W. Zhao, Z. B. Wang and W. Wang, Effect of gradient nanostructured Ti on behaviours of MG63 cells in vitro, Journal of Nanomaterials, **12**, 2020, 1–11.
11 Y. Zhu, C. N. Zhang, Y. X. Gu, J. Y. Shi, J. J. Mo, S. J. Qian, S. C. Qiao and H. C. Lai, The responses of human gingival fibroblasts to magnesium-doped titanium, *J. Biomed. Mater. Res.*, 2020, **108**, 267–278.
12 H. L. Cao, K. W. Tang and X. Y. Liu, Bifunctional galvanics mediated selective toxicity on titanium, *Mater. Horiz.*, 2018, **5**, 264–267.
13 R. Huang, Y. Han and S. M. Lu, Enhanced osteoblast functions and bactericidal effect of Ca and Ag dual-ion implanted surface layers on nanograined titanium alloys, *J. Mater. Chem. B*, 2014, **2**, 4531–4543.
14 T. Lu, S. Qian, F. H. Meng, C. Q. Ning and X. Y. Liu, Enhanced osteogenic activity of poly ether ether ketone

using calcium plasma immersion ion implantation, *Colloids Surf., B*, 2016, **142**, 192–198.

15 S. N. Nayab, F. H. Jones and I. Olsen, Modulation of the human bone cell cycle by calcium ion- implantation of titanium, *Biomaterials*, 2007, **28**, 38–44.

16 J. H. Liang, R. Song, Q. L. Huang, Y. Yang, L. X. Lin, Y. M. Zhang, P. L. Jiang, H. P. Duan, X. Dong and C. J. Lin, Electrochemical construction of a bio-inspired micro/nano-textured structure with cell-sized microhole arrays on biomedical titanium to enhance bioactivity, *Electrochim. Acta*, 2015, **174**, 1149–1159.

17 J. F. Liang, S. S. Xu, M. M. Shen, B. K. Cheng, Y. F. Li, X. W. Liu, D. Z. Qin, A. Bellare and L. Kong, Osteogenic activity of titanium surfaces with hierarchical micro-/nano-structures obtained by hydrofluoric acid treatment, *Int. J. Nanomed.*, 2017, **12**, 1317–1328.

18 W. Sun, D. Ma, J. G. M. Bolscher, K. Nazmi, E. C. I. Veerman, F. J. Bikker, P. Sun, H. Y. Lin and G. Wu, Human salivary histatin-1 promotes osteogenic cell spreading on both bio-inert substrates and titanium SLA surfaces, *Front. Bioeng. Biotechnol.*, 2020, **8**, 584410.

19 Y. Y. Guo, B. B. Hu, C. Tang, Y. P. Wu, P. F. Sun, X. L. Zhang and Y. H. Jia, Increased osteoblast function *in vitro* and *in vivo* through surface nanostructuring by ultrasonic shot peening, *Int. J. Nanomed.*, 2015, **10**, 4593–4603.

20 W. T. Huo, L. Z. Zhao, W. Zhang, J. W. Lu, Y. Q. Zhao and Y. S. Zhang, In vitro corrosion behavior and biocompatibility of nanostructured Ti6Al4V, *Mater. Sci. Eng., C*, 2018, **92**, 268–279.

21 C. L. Zhao, P. Cao, W. P. Ji, P. Han, J. H. Zhang, F. Zhang, Y. Jiang and X. N. Zhang, Hierarchical titanium surface textures affect osteoblastic functions, *J. Biomed. Mater. Res.*, 2011, **99**, 666–675.

22 J. Sun, Q. T. Yao, Y. H. Zhang, X. D. Du, Y. C. Wu and W. P. Tong, Simultaneously improving surface mechanical properties and *in vitro* biocompatibility of pure titanium *via* surface mechanical attrition treatment combined with low-temperature plasma nitriding, *Surf. Coat. Technol.*, 2017, **309**, 382–389.

23 S. Bahl, B. T. Aleti, S. Suwas and K. Chatterjee, Surface nanostructuring of titanium imparts multifunctional properties for orthopedic and cardiovascular applications, *Mater. Des.*, 2018, **144**, 169–181.

24 W. Wang, Z. B. Wang, Y. T. Fu, N. Dunne, C. Liang, X. Luo, K. D. Liu, X. M. Li, X. N. Pang and K. Lu, Improved osteogenic differentiation of human amniotic mesenchymal stem cells on gradient nanostructured Ti surface, *J. Biomed. Mater. Res.*, 2020, **108**, 1824–1833.

25 C. L. Zhao, W. P. Ji, P. Han, J. H. Zhang, Y. Jiang and X. N. Zhang, *In vitro* and *in vivo* mineralization and osseointegration of nanostructured Ti6Al4V, *J. Nanopart. Res.*, 2011, **13**, 645–654.

26 C. L. Zhao, P. Han, W. P. Ji and X. N. Zhang, Enhanced mechanical properties and *in vitro* cell response of surface mechanical attrition treated pure titanium, *J. Biomater. Appl.*, 2010, **27**, 113–118.

27 M. Lai, K. Y. Cai, Y. Hu, X. F. Yang and Q. Liu, Regulation of the behaviors of mesenchymal stem cells by surface nanostructured titanium, *Colloids Surf., B*, 2012, **97**, 211–220.

28 R. Huang, H. Y. Zhuang and Y. Han, Second-phase-dependent grain refinement in Ti-25Nb-3Mo-3Zr-2Sn alloy and its enhanced osteoblast response, *Mater. Sci. Eng., C*, 2014, **35**, 144–152.

29 L. Y. Wang, J. J. Qiu, S. Qian and X. Y. Liu, Interface effects on regulating the behaviors of human gingival fibroblasts on titanium by Zn-PIII, *Surf. Coat. Technol.*, 2020, **403**, 126357.

30 Y. R. Yan, Y. Wei, R. Yang, L. Xia, C. C. Zhao, B. Gao, X. M. Zhang, J. J. Fu, Q. Wang and N. Xu, Enhanced osteogenic differentiation of bone mesenchymal stem cells on magnesium-incorporated titania nanotube arrays, *Colloids Surf., B*, 2019, **179**, 309–316.

31 T. Wang, Y. Wan and Z. Q. Liu, Synergistic effects of bioactive ions and micro/nano-topography on the attachment, proliferation and differentiation of murine osteoblasts (MC3T3), *J. Mater. Sci.: Mater. Med.*, 2016, **27**, 133.

32 L. Li, L. T. Yao, H. Y. Wang, X. F. Shen, W. W. Lou, C. Y. Huang and G. Wu, Magnetron sputtering of strontium nanolayer on zirconia implant to enhance osteogenesis, *Mater. Sci. Eng., C*, 2021, **127**, 112191.

33 K. H. Ko, D. G. Kim, H. Lee, E. Byon, Y. Jeong, C. J. Park and L. R. Cho, Gene expression in Ca or Mg implanted titanium surfaces, *Tissue Eng. Regener. Med.*, 2012, **9**, 137–146.

34 I. Shabani, V. Haddadi-Asl, M. Soleimani, E. Seyedjafari and S. M. Hashemi, Ion-exchange polymer nanofibers for enhanced osteogenic differentiation of stem cells and ectopic bone formation, *ACS Appl. Mater. Interfaces*, 2014, **6**, 72–82.

35 A. I. Rodrigues, M. B. Oliveira, J. F. Mano, M. E. Gomes, R. L. Reis and I. B. Leonor, Combinatorial effect of silicon and calcium release from starch-based scaffolds on osteogenic differentiation of human adipose stem cells, *ACS Biomater. Sci. Eng.*, 2015, **1**, 760–770.

36 Y. T. Xie, X. Y. Liu, P. K. Chu and C. X. Ding, Nucleation and growth of calcium-phosphate on Ca-implanted titanium surface, *Surf. Sci.*, 2006, **600**, 651–656.

37 D. Krupa, J. Baszkiewicz, B. Rajchel, A. Barcz, J. W. Sobczak, A. Bilinski and T. Borowski, Effect of calcium-ion implantation on the corrosion resistance and bioactivity of the Ti6Al4V alloy, *Vacuum*, 2007, **81**, 1310–1313.

38 X. Y. Liu, R. W. Y. Poon, S. C. H. Kwok, P. K. Chu and C. X. Ding, Structure and properties of Ca-plasma-implanted titanium, *Surf. Coat. Technol.*, 2005, **191**, 43–48.

39 X. Y. Liu, R. W. Y. Poon, S. C. H. Kwok, P. K. Chu and C. X. Ding, Plasma surface modification of titanium for hard tissue replacements, *Surf. Coat. Technol.*, 2004, **186**, 227–233.

40 D. Krupa, J. Baszkiewicz, J. A. Kozubowski, A. Barcz, J. W. Sobczak, A. Bilinski, M. Lewandowska-Szumiel and B. Rajchel, Effect of calcium-ion implantation on the corrosion resistance and biocompatibility of titanium, *Biomaterials*, 2001, **22**, 2139–2151.

41 S. N. Nayab, F. H. Jones and I. Olsen, Effects of calcium ion implantation on human bone cell interaction with titanium, *Biomaterials*, 2005, **26**, 4717–4727.
42 C. Hegedus, C. C. Ho, A. Csik, S. Biri and S. J. Ding, Enhanced physicochemical and biological properties of ion-implanted titanium using electron cyclotron resonance ion sources, *Materials*, 2016, **9**, 25.
43 S. N. Nayab, F. H. Jones and I. Olsen, Effects of calcium ion-implantation of titanium on bone cell function in vitro, *J. Biomed. Mater. Res.*, 2007, **83**, 296–302.
44 S. Won, Y. H. Huh, L. R. Cho, H. S. Lee, E. S. Byon and C. J. Park, Cellular response of human bone marrow derived mesenchymal stem cells to titanium surfaces implanted with calcium and magnesium ions, *Tissue Eng. Regener. Med.*, 2017, **14**, 123–131.
45 R. Sawada, K. Kono, K. Isama, Y. Haishima and A. Matsuoka, Calcium-incorporated titanium surfaces influence the osteogenic differentiation of human mesenchymal stem cells, *J. Biomed. Mater. Res.*, 2013, **101**, 2573–2585.
46 Z. T. Yu and L. Zhou, Influence of martensitic transformation on mechanical compatibility of biomedical β type titanium alloy TLM, *J. Mater. Sci. Eng. A*, 2006, **438–440**, 391–394.
47 R. Huang, L. Zhang, L. Huang and J. X. Zhu, Enhanced in-vitro osteoblastic functions on β-type titanium alloy using surface mechanical attrition treatment, *Mater. Sci. Eng., C*, 2019, **97**, 688–697.
48 S. S. Sidhu, H. Singh and M. A. Gepreel, A review on alloy design, biological response, and strengthening of β-titanium alloys as biomaterials, *Mater. Sci. Eng., C*, 2021, **121**, 111661.
49 K. Lu and J. Lu, Nanostructured surface layer on metallic materials induced by surface mechanical attrition treatment, *J. Mater. Sci. Eng. A*, 2004, **375–377**, 38–45.
50 X. Wu, N. Tao, Y. Hong, B. Xu, J. Lu and K. Lu, Microstructure and evolution of mechanically- induced ultrafine grain in surface layer of AL-alloy subjected to USSP, *Acta Mater.*, 2002, **50**, 2075–2084.
51 S. Bagherifard, D. J. Hickey, A. C. Luca, V. N. Malheiro, A. E. Markaki, M. Guagliano and T. J. Webster, The influence of nanostructured features on bacterial adhesion and bone cell functions on severely shot peened 316L stainless steel, *Biomaterials*, 2015, **73**, 185–197.
52 S. Bagherifard, S. Slawik, I. Fernandez-Pariente, C. Pauly, F. Mucklich and M. Guagliano, Nanoscale surface modification of AISI 316L stainless steel by severe shot peening, *Mater. Des.*, 2016, **102**, 68–77.
53 T. Kokubo and H. Takadama, How useful is SBF in predicting *in vivo* bone bioactivity?, *Biomaterials*, 2006, **27**, 2907–2915.
54 Y. Han, D. Chen, J. Sun, Y. Zhang and K. Xu, UV-enhanced bioactivity and cell response of micro-arc oxidized titania coatings, *Acta Biometer.*, 2008, **4**, 1518–1529.
55 Y. Han, J. H. Zhou, S. M. Lu and L. Zhang, Enhanced osteoblast functions of narrow interligand spaced Sr-HA nano-fibers/rods grown on microporous titania coatings, *RSC Adv.*, 2013, **3**, 11169–11184.
56 J. W. Park, Y. J. Kim, C. H. Park, D. H. Lee, Y. G. Ko, J. H. Jang and C. S. Lee, Enhanced osteoblast response to an equal channel angular pressing-processed pure titanium substrate with microrough surface topography, *Acta Biomater.*, 2009, **5**, 3272–3280.
57 P. Jojibabu, B. R. Sunil, T. S. S. Kumar, U. Chakkingal, V. Nandakumar and M. Doble, Wettability and *in vitro* bioactivity studies on titanium rods processed by equal channel angular pressing, *Trans. Indian Inst. Met.*, 2013, **66**, 299–304.
58 C. Gurau, G. Gurau, V. Mitran, A. Dan and A. Cimpean, The influence of severe plastic deformation on microstructure and *in vitro* biocompatibility of the new Ti-Nb-Zr-Ta-Fe-O alloy composition, *Materials*, 2020, **13**, 4853.
59 S. Faghihi, A. P. Zhilyaev, J. A. Szpunar, F. Azari, H. Vali and M. Tabrizian, Nanostructuring of a titanium material by high-pressure torsion improves pre-osteoblast attachment, *Adv. Mater.*, 2007, **19**, 1069–1073.
60 R. Huang, L. Liu, B. Li, L. Qin, L. Huang, K. W. K. Yeung and Y. Han, Nanograins on Ti-25Nb-3Mo-2Sn-3Zr alloy facilitate fabricating biological surface through dual-ion implantation to concurrently modulate the osteogenic functions of mesenchymal stem cells and kill bacteria, *J. Mater. Sci. Technol.*, 2021, **73**, 31–44.
61 A. R. Pandey, D. Rai, S. P. Singh, A. K. Tripathi, A. Sardar, A. Ansari, A. Mishra, S. Bhagwati, R. S. Bhatta, M. I. Siddiqi, N. Chattopadhyay, R. Trivedi and K. V. Sashidhara, Synthesis and evaluation of galloyl conjugates of flavanones as BMP-2 upregulators with promising bone anabolic and fracture healing properties, *J. Med. Chem.*, 2021, **64**, 12487–12505.
62 Q. Lei, J. Chen, W. X. Huang, D. Wu, H. Z. Lin and Y. Z. Lai, Proteomic analysis of the effect of extracellular calcium ions on human mesenchymal stem cells: Implications for bone tissue engineering, *Chem.-Biol. Interact.*, 2015, **233**, 139–146.
63 M. N. Lee, H. S. Hwang, S. H. Oh, A. Roshanzadeh, J. W. Kim, J. H. Song, E. S. Kim and J. T. Koh, Elevated extracellular calcium ions promote proliferation and migration of mesenchymal stem cells *via* increasing osteopontin expression, *Exp. Mol. Med.*, 2018, **50**, 142–157.
64 A. M. C. Barradas, H. A. M. Fernandes, N. Groen, Y. C. Chai, J. Schrooten, J. V. D. Peppel, J. P. T. M. V. Leeuwen, C. A. V. Blitterswijk and J. D. Boer, A calcium-induced signaling cascade leading to osteogenic differentiation of human bone marrow-derived mesenchymal stromal cells, *Biomaterials*, 2012, **33**, 3205–3215.
65 B. Setzer, M. Bachle, M. C. Metzger and R. J. Kohal, The gene-expression and phenotypic response of hFOB 1.19 osteoblasts to surface-modified titanium and zirconia, *Biomaterials*, 2009, **30**, 979–990.